Astron. Astrophys. 334, 713–728 (1998)

ASTRONOMY AND ASTROPHYSICS

Bolides produced by impacts of large meteoroids into the Earth's atmosphere: comparison of theory with observations

I. Benešov bolide dynamics and fragmentation

J. Borovička[1], O.P. Popova[2], I.V. Nemtchinov[2], P. Spurný[1], and Z. Ceplecha[1]

[1] Ondřejov Observatory, Astronomical Institute of the Academy of Sciences, CZ-251 65 Ondřejov, Czech Republic
[2] Institute for Dynamics of Geospheres, Russian Academy of Sciences, Leninsky pr. 38, build. 6, 117979 Moscow, Russia

Received 23 September 1997 / Accepted 12 January 1998

Abstract. Detailed analysis of one of the largest and well documented bolides – the Benešov bolide (EN 070591) – has been performed. The bolide had an initial velocity of 21 km s^{-1}, reached a maximal absolute magnitude of -19.5 at the altitude of 24 km and radiated down to 17 km. Detailed photographic data for the light curve, geometry and dynamics of the main body and several fragments are available. This enabled us to test the theoretical radiative-hydrodynamic model used previously for the analysis of satellite-detected bolides.

The conventional analysis produces a huge discrepancy between the dynamic (80–300 kg) and photometric (5000–13,000 kg) mass. The discrepancy might be removed assuming a low density of 0.5 g cm^{-3} but this is unrealistic. The radiative-hydrodynamic modeling yielded a mass of 2000 kg and density of 1–2 g cm^{-3}. However, the dynamics was not sufficiently well reproduced.

There is direct observational evidence of meteoroid fragmentation at altitudes of 38–31 km and of catastrophic disruption at 24 km. These, however, do not explain the problem with the mass. The crucial point is that the bolide was significantly decelerated already at the altitudes between 50–40 km, while enormous luminosity was produced below 40 km. We suggest that the meteoroid must have been fragmented into 10–30 pieces of a mass of 100–300 kg already at an altitude of 60–50 km. By creating a progressive fragmentation model with two types of fragmentation at three different altitude levels, we were able to reproduce the dynamics and luminosity sufficiently well. The best estimate of the initial mass is 3000–4000 kg for a density of 2 g cm^{-3}.

The comparison with the bolide PN 39434 suggests that the behavior of Benešov is typical for large stony meteoroids. Early fragmentation under dynamic pressures of the order of 1 Mdyn cm^{-2} is very important. The analysis of the light curve with the radiative-hydrodynamic model can give good order-of-magnitude estimates of mass, if no dynamic data are available.

Key words: meteoroids, meteors

Send offprint requests to: J. Borovicka, (borovic@asu.cas.cz)

1. Introduction

The atmospheric entry of a large meteoroid is associated with intense radiation. The characteristics of the bolide (the energy of the light flash, its duration, the shape of the light curve) may be used for the assessment of the meteoroid characteristics, e.g. its kinetic energy. Bolide spectra may give important information on the chemical composition of the meteoroids and the conditions at which the plasma emits radiation (its temperature, density, degree of equilibrium).

Large meteoroid impacts are relatively rare and the ground based photographic networks gather the detailed data rather slowly. This resulted in great interest in the analysis of very bright meteors detected by the European Fireball Network (EN), i.e. Benešov and Šumava (Spurný 1994; Borovička & Spurný 1996). Preliminary estimates of the masses of these bolides were 5–15 tons (the kinetic energy equivalent to the energy of about 200–600 tons TNT). Satellite-based photoelectric sensors (Tagliaferri et al. 1994) have detected a large number of bright flashes caused by the entry and disintegration of large meteoroids in the Earth's atmosphere. Initial kinetic energies of these meteoroids are equivalent to the energy of 0.05–40 kt TNT (Nemtchinov et al. 1997). For the typical velocities of 15–20 km s^{-1}, this corresponds to masses in the range of 1–1000 tons. Thus, the energy of Benešov and Šumava are near the lower sensitivity limit of the satellite-based network.

The Satellite Network (SN) system does not measure the velocity on the trajectory as yet, so dynamical analysis is not possible. For Benešov and Šumava we do have data on the trajectory, velocity, light curve, fragmentation points and even on the spectrum. This enables us to apply the methods developed for the analysis of smaller meteoroids registered by the European Network (EN) and Prairie Network (PN). The methods include the gross-fragmentation model of Ceplecha et al. (1993) and the spectral model of Borovička (1993).

For the SN bolides, analysis of the light curve is the only possibility. The classical theory of meteor phenomena (for a review see e.g. Bronsten 1983) assumes that the amount of emitted energy per unit time is proportional to the kinetic energy of the mass losses due to ablation. More generally, the emitted energy

is proportional to the energy deposition into the atmosphere during the meteoroid flight (ReVelle 1979, 1980). The coefficient of proportionality (luminous efficiency) is an empirical constant, determined from the experiments with artificial meteors created by small, gram-sized high-velocity projectiles (Givens & Page 1971) or from the analysis of meteors in which not only the light curve was measured, but characteristics of a meteoroid (e.g. Innisfree and Lost City) were estimated using some kind of trajectory analysis combined with data on the recovered meteorites (Halliday et al. 1981; Ceplecha 1987, 1996).

There is a great scatter in the empirical values of luminous efficiency probably caused by the differences in size, shape, velocity, strength and composition of the meteoroid. One cannot use a single value of luminous efficiency determined in a limited number of events for all the meteoroids, especially for very bright bolides. For large meteoroids the optical thickness of the shock-heated air and meteoroid vapor stream formed due to ablation is rather large. In contrast, for very small meteoroids the air and vapor plasma is optically thin. Moreover, the luminous efficiency depends on the spectral sensitivity of the sensor used and one cannot simply take the data obtained in a photographic observations and use them in the interpretation of photoelectric measurements and vice versa without caution. Thus there exists an acute necessity of a theory of the luminous processes for large meteoroids.

An attempt to create such a theory has been made in a paper by Nemtchinov et al. (1994). A border case of a very large body has been considered. In that case the optical thickness of the shock-heated air is so large that no vapor radiation escapes from the head of the bolide. The temperature characterizing the spectrum of the radiation is rather high, although lower than the temperature near the stagnation point of the blunt nose of a meteoroid, which is about 20,000 K. Such large bolides, e.g. with a size of about 30–100 m, should be considered as possible hazardous objects (Morrison et al. 1994; Adushkin & Nemtchinov 1994; Nemtchinov et al. 1996), but happily have not impacted the Earth for a long time, at least not in this century with the possible exception of the Tunguska event in 1908.

For smaller bodies which enter the Earth's atmosphere much more frequently (of e.g. 1–10 cm), the role of the air radiation is under suspicion. Meteor spectra in the spectral range of ground-based observations are dominated by the vapor lines and the characteristic temperature is only about 4000 K (Borovička 1993). The second component of about 10,000 K consists of only few lines. This component is faint in slow meteors but relatively bright in meteors of high velocity and contains also several atmospheric lines, especially in the infrared (Borovička 1994).

Observations clearly show that vapor radiation dominates at least for meteoroids smaller than $\sim$ 1 m. To describe meteor radiation for meteoroids of various sizes taking into account radiation transfer both in the air and in the vapor, a radiative-hydrodynamic model has been developed (Golub' et al. 1996a). The emerging spectral radiation was computed and self-consistent values of luminous efficiency and ablation rate were calculated for different sizes, velocities, altitudes of flight and meteoroid composition. The model has then been used to analyze bolide light curves using the so called radiative radius approach. The observed luminosity was related to an effective radius causing the same luminosity (Nemtchinov et al. 1994, 1995, 1997; Popova & Nemtchinov 1996a).

The verification of this theoretical model is the main subject of this paper and two subsequent papers. Here we analyze the dynamics, light curve and fragmentation of the Benešov bolide. The theoretical model is described in more detail in Sect. 2. In Sect. 3, the model is applied to the Benešov bolide and compared with the analysis done with the Ceplecha et al. (1993) gross-fragmentation model. The discrepancies found are discussed in Sects. 4 and 5. The next paper will be devoted to the analysis of Benešov bolide spectrum. The last paper of the series will be devoted to the Šumava bolide, a bolide with quite different characteristics than Benešov.

2. Theoretical model

2.1. Luminous efficiencies and ablation coefficients

The luminous efficiencies and ablation coefficients used here for the Benešov bolide modeling are taken from the radiative-hydrodynamic model of Golub' et al. (1996a, 1997). Radiation transfer in the air and in the meteoritic vapor has been taken into account. The model is based on the analogy between one-dimensional nonstationary motion of a cylindrical piston in the air and the two-dimensional quasistationary flow around the body (Chernyi 1959; Hayes & Probstein 1959). Detailed tables of the spectral opacities of iron and chondrite vapors published by Kosarev et al. (1996) were used. The same data were used for the analysis of the PN bolides (Popova & Nemtchinov 1996a) and SN bolides (Nemtchinov et al. 1995, 1997). Luminous coefficients in the wavelength range of ground-based optical observations are given in Table 1. The ablation coefficient σ which determines the decrease of meteoroid mass with the decrease of its velocity is presented in Table 2.

It is interesting to note that total radiation losses for large (with sizes of about 10 cm and larger) iron and H-chondrites and other meteoroids with rather high iron content do not differ substantially (no more than by a factor of two or three) from those of a pure silica body or from values obtained in a framework of an air-radiation dominated model. This is explained by the fact that the radiation of the vapor in the ablating piston model is substantially governed by the radiation emitted by the shock-heated air, absorbed and re-emitted by the vapor. But we should keep in mind that the spectrum may be substantially different and luminous efficiencies in different wavelength ranges (i.e. for different types of sensors) may differ drastically (Golub' et al. 1996b, 1997).

The luminous efficiencies in Table 1 agree to within an order of magnitude with the empirical values obtained from the analysis of the photographed meteorite falls (Halliday et al. 1981; Ceplecha 1996).

The values of σ in Table 2 are about an order of magnitude higher than those computed for smooth spherical bodies covered

Table 1. Fraction of radiative energy emitted in photon energy range 1.88–3.44 eV of the total energy contributed into the air

Height	Velocity	Radius		
km	km s^{-1}	0.14 m	1.4 m	14 m
50	30	0.30	0.057	0.13
	20	0.013	0.036	0.077
	15	0.0074	0.020	0.056
	12	0.0052	0.0081	0.030
	10	0.0048	0.0040	0.018
40	30	0.038	0.085	0.17
	20	0.026	0.061	0.13
	15	0.01	0.036	0.095
	12	0.0069	0.018	0.059
	10	0.0038	0.0068	0.025
30	30	0.066	0.12	0.14
	20	0.041	0.098	0.14
	15	0.028	0.069	0.11
	12	0.016	0.038	0.076
	10	0.0083	0.015	0.046
20	30	0.097	0.14	0.15
	20	0.075	0.11	0.14
	15	0.049	0.069	0.11
	12	0.025	0.040	0.078
	10	0.011	0.024	0.064

Table 2. Ablation coefficient [s^2 km^{-2}] from the model

Height	Velocity	Radius		
km	km s^{-1}	0.14 m	1.4 m	14 m
50	30	0.020	0.0094	0.0065
	20	0.023	0.012	0.0094
	15	0.014	0.012	0.010
	12	0.012	0.0076	0.0069
	10	0.012	0.0076	0.0046
40	30	0.0094	0.0049	0.0026
	20	0.013	0.0075	0.0052
	15	0.012	0.0078	0.0059
	12	0.0078	0.0050	0.0058
	10	0.0078	0.0041	0.0038
30	30	0.0040	0.0022	0.0011
	20	0.0056	0.0038	0.0017
	15	0.0063	0.0049	0.0024
	12	0.0045	0.0042	0.0024
	10	0.0031	0.0027	0.0023
20	30	0.0017	0.0009	0.00025
	20	0.0025	0.0011	0.00036
	15	0.0031	0.0016	0.00055
	12	0.0025	0.0016	0.00071
	10	0.0018	0.0015	0.00078

with a special thermal shielding (Biberman et al. 1980). They agree with the range of empirical values of σ for meteoritic bodies of small sizes (ReVelle 1979, 1980; Bronsten 1983).

It is interesting to compare in more detail the resulting ablation coefficients with those determined with the help of a substantially different method. The gross-fragmentation model (Ceplecha et al. 1993) was applied to 43 PN bolides (Ceplecha et al. 1996). In this dynamical method, the observed length and height are fitted as a function of time. The ablation coefficient is a free parameter and is assumed constant along the whole trajectory. However, only the part of the trajectory where the body is being decelerated significantly is crucial for the determination of the ablation coefficient. This part always lies near the end of the trajectory, typically at heights below 40 km.

Different groups of meteoroids were recognized by Ceplecha & McCrosky (1976) on the basis of their penetration ability into the Earth's atmosphere. The existence of the groups was confirmed also from the distribution of ablation coefficients (Ceplecha et al. 1993). A typical value of the ablation coefficient is 0.01 s^2 km^{-2} for group I (ordinary chondrites) and 0.04 s^2 km^{-2} for group II (carbonaceous chondrites). These values can be compared with the ablation coefficients from Table 2 below 40 km. The latter coefficients decrease with meteoroid size. The ablation parameters σ for meteoroids with a radius of about 14 cm at an altitude of 40 km are close to Ceplecha's estimates for H-chondrite bodies (meteoroid of type I according to his classification). For type II meteoroids the estimates of Ceplecha et al. (1996) are higher: $\sigma \approx 0.022$–$0.053\,s^2\,km^{-2}$. When the altitude decreases, theoretical ablation parameters also decrease and are lower than the average Ceplecha estimates (0.01 s^2 km^{-2} for type I) by a factor of 3–5 at 20 km altitude and by a factor of 1.5–3 times at 30 km altitude. Possibly, some additional ablation processes must be taken into account at low heights.

In the ablating piston model (Golub' et al. 1996a) mass losses are dominated by vaporization due to thermal radiation falling onto the surface of a meteoroid. The ablation process was assumed to take place uniformly over the surface of a meteoroid in accordance with the value of the radiation flux. Melting, and shedding of the melted layer, are also incorporated into the model. The mass loss rate due to the shedding of a melting layer is estimated assuming that the melting layer gradually flows along the surface of a meteoroid under the pressure gradient. Separate vaporization of inclusions with a low vaporization temperature and low specific energy of vaporization and an increase of shedding due to roughness of the surface and rapid evaporation of inclusions have not been taken into account.

There are some other known limitations of the theory under consideration. A strict boundary between vapor and air is assumed. But in reality this boundary is unstable and large-eddy and small-scale turbulent mixing of the vapor and air may occur. This effect is now being included into a modified ablating piston model (A.P. Golub', personal communication), but no numerical calculations have been obtained as yet. At the present stage of investigation the tabulated theoretical luminous efficiencies and ablation coefficients are used to analyze bolide light curves.

2.2. Radiative radius approach

In the radiative radius approach (Nemtchinov et al. 1994, 1995, 1997), the radius is defined from the light curve. The simplest way to determine the size of the body at any moment is to compare the observed intensity with the theoretical values for different sizes for the given velocity and at the altitude under consideration and to chose one which gives the best fit of radiation intensity to the light curve.

Assuming some shape of the body and a value of the bulk density it is easy to obtain the mass of the meteoroid. But to use this estimate (we call it model R) one needs information on the velocity of the meteoroid versus altitude and on the breakup points. Such information is available for the Prairie Network (PN) and European Network (EN) bolides.

For the case of the satellite observational system in most cases trajectory tracking has not been done as yet. In this case another technique has been used (Svetsov et al. 1995). Indirect integration of the system of equations of meteoroid motion, ablation and radiation allows us to obtain the initial parameters. The functions $m(t), R(t), v(t)$ and $h(t)$ (mass, radius, velocity and height as a function of time) may be found, if we use the initial velocity as initial data and the height at peak signal and the velocity at the end of the radiation impulse as boundary conditions. A numerical solution can be calculated by an iterative procedure. The values of initial mass and size at the beginning of the light signal follow from the numerical solution. A precise value of the terminal velocity is of little importance, because the main part of the numerical solution is not appreciably influenced by its value for most of the bolides. The coefficients of ablation and luminosity are calculated beforehand and are considered as given functions of radius, height, velocity, and assumed type of meteoroid.

Obtaining the initial mass and size from the solution, we can assess the initial density of the body, assuming that the meteoroid is not very elongated or very flattened. For the Benešov bolide we shall calculate masses using this estimate (S model) and estimate R – and of course the usual dynamic mass and compare them. Model S is in fact a combination of the instantaneous radiation radius technique (model R) and the usual dynamic method.

Comparison of the ablation piston model with observations for some of the PN bolides was already given in Popova & Nemtchinov (1996a). The light intensity depends substantially on the type of fragmentation. If a small number of large fragments are formed and they diverge due to aerodynamic forces between them (Passey & Melosh 1980; Artem'eva & Shuvalov 1996) after a short period of interaction between the fragments they begin to move and emit radiation independently. There is no substantial increase in the intensity and the radiation radius.

If a large number of fragments is formed, the smallest fragments rapidly evaporate, and a cloud of fragments and vapor, bounded by a common bow shock-wave, expands under aerodynamic forces acting on the leading edge of the cloud (Svetsov et al. 1995). The result is an intense flash. In this case fragmentation is taken into account in a simplified manner. For the cloud of fragments and vapor the same single-body model is used as for the unfragmented body. A rapid increase in the size of the cloud of small fragments and vapor was modeled in the framework of a liquid-like model. The size of a cloud giving the same light intensity as the observed cloud is the radiative radius. The dependence of this radius on the altitude is the result of observations. Of course, intermediate regions may exist, e.g. at the first breakup only large fragments are formed but later gross-fragmentation may follow. It is difficult to predict which type of fragmentation will occur in a particular event and additional analysis of the observational data is necessary.

3. Analysis of the Benešov bolide with the radiative radius model

The Benešov bolide (EN 070591) entered the atmosphere almost vertically with an initial velocity of about 21 km s^{-1} and reached a maximum absolute stellar magnitude of -19.5 mag (Borovička & Spurný 1996). It penetrated deeply into the atmosphere; the last point at which the velocity of one of the fragments has been determined (5 km s^{-1}) is at 19 km. The type of fragmentation accompanied by obvious brightening of the bolide (similar to observed for SN bolides) was registered during the flight. Several fragmentation events were directly visible on the photographs (Spurný 1994). The trajectories of the fragments deviating slightly from the main trajectory could be directly measured (Borovička & Spurný 1996).

The Benešov bolide was simulated using the radiative radius approach in the same way as has been done for satellite registered (SN) bolides (Svetsov et al. 1995; Nemtchinov et al. 1994, 1997). Unlike the SN bolides, not only the light curve and height of maximum intensity, but also the trajectory slope and initial and terminal velocities are well known for Benešov from the observations. The light curve is shown in Fig. 1a. Only the heights below 50 km, where the simulations were done, are shown. The quasi periodic fluctuations obvious especially at the beginning of the light curve are an artifact caused by the rotating shutter.

The resulting effective radiative radius as a function of height is shown in Fig. 1b. The radius shows two major maxima – the main at an altitude of about 24 km and other below 40 km, at altitudes of 38–31 km. A substantial increase of radiative radius is interpreted in the model as fragmentation of the meteoroid creating a cloud of vapor and small fragments. The intervals in which the radiative radius increases really correspond with the observed fragmentation events (see below).

The calculated decrease of mass with height is shown in Fig. 1d. The initial mass estimate is about 2000 kg. This is lower than the estimate of Borovička & Spurný (1996), i.e. $M \sim$ 5000–13,000 kg. The high value of the terminal mass (about 1000 kg) is probably due to an underestimation of theoretical ablation rates below 30 km (Popova & Nemtchinov 1996a). An artificial increase of these rates close to their quasi-empirical values (Ceplecha et al. 1993) does not change the initial mass estimate but decreases the end mass value by a factor of two to three.

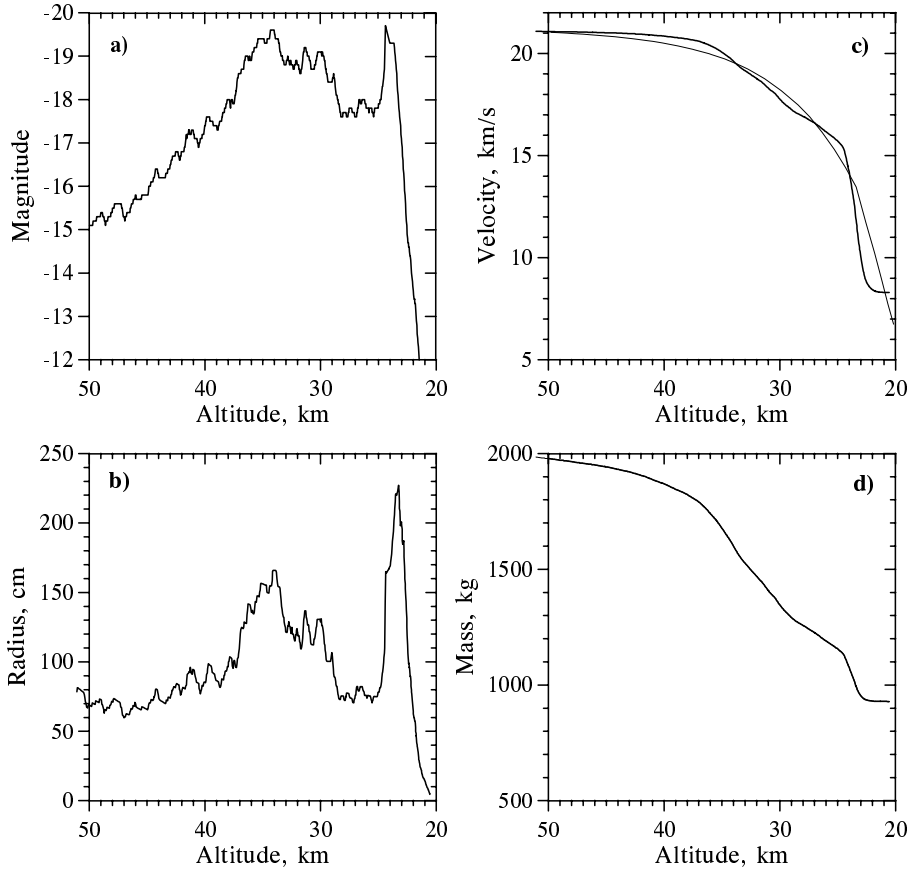

Fig. 1a–d. Numerical simulation of the light curve of the Benešov bolide by the radiative radius model: **a** observed light curve, **b** simulated radiative radius, **c** simulated velocity (thick line), **d** simulated mass. The velocity curve obtained as a result of fitting observational data by the gross-fragmentation model is shown as the thin line in panel c

The density of the meteoroid, calculated from the mass and effective radius before the fragmentation, seems to be about 1–2 g cm^{-3}. The density determination in this model is slightly uncertain because it depends on the assumed shape and the drag coefficients. The estimate R may be used for the Benešov bolide only above 40 km, as below this altitude fragmentation is evident. It allows us to obtain a meteoroid mass of about 2000–4000 kg for an assumed density of 2 g cm^{-3} or 4000–8000 kg for $\rho = 3.7$ g cm^{-3}. These values are close to the photometric mass and substantially greater than the dynamic mass. This divergence will be discussed below.

The radiative radius model can be checked by comparison of the predicted and observed deceleration along the trajectory. The deceleration curve was obtained from observations with the help of the gross-fragmentation model of Ceplecha et al. (1993). The time-length data along the bolide trajectory below altitude 50 km were fitted to obtain the best solution. This procedure revealed the main fragmentation point as discussed below. The resulting deceleration curve is shown by the thin line in Fig. 1c – the theoretical curve based on the radiative radius approach is given by the thick line.

The curves coincide rather well above an altitude of 24 km, where the catastrophic disruption of the body occurred. The more rapid velocity decrease below 24 km for the theoretical model is caused by the creation of a spreading cloud of vapor and small fragments in the last gross-fragmentation. The end of the observed light curve and deceleration curve after the flare relates to fragments which survived the disruption. They continue their ways independent from each other and this leads to violation of the single-body model used in the simulation. Exclusion of the last points on the light curve from the simulation allows us to get a better termination of the velocity and mass dependencies.

To compare the model results directly with observations, length as a function of time along the meteoroid trajectory was determined (Fig. 2). The thick line shows the difference between the observed ($l_{\rm obs}$) and computed ($l_{\rm com}$) lengths for the theoretical radiative radius model. The thin line is a result of the application of the gross-fragmentation model mentioned above. In the latter model the observed lengths are directly fitted, so the residuals $l_{\rm obs} - l_{\rm com}$ show only random variations caused by the inaccuracy of the measurements. The standard deviation of one measurement is 17 meters.

The radiative radius model shows larger deviations. Apart from the main difference below 24 km discussed above, a smaller deviation is observed also at the time 0.7–1.0 s corresponding to altitudes 36–31 km. (Time is counted here from the beginning of the simulations at altitude 51.2 km). This deviation reaches about 150 m at maximum which is not a particularly large value, nevertheless it is significant. The deviation demonstrates the fact that the meteoroid was being decelerated between the altitudes 50–37 km more than predicted in the model (see also Fig. 1c). At altitudes around 35 km, the increasing effective radius caused more deceleration in the model, the predicted velocity decreased and the length difference began to decrease.

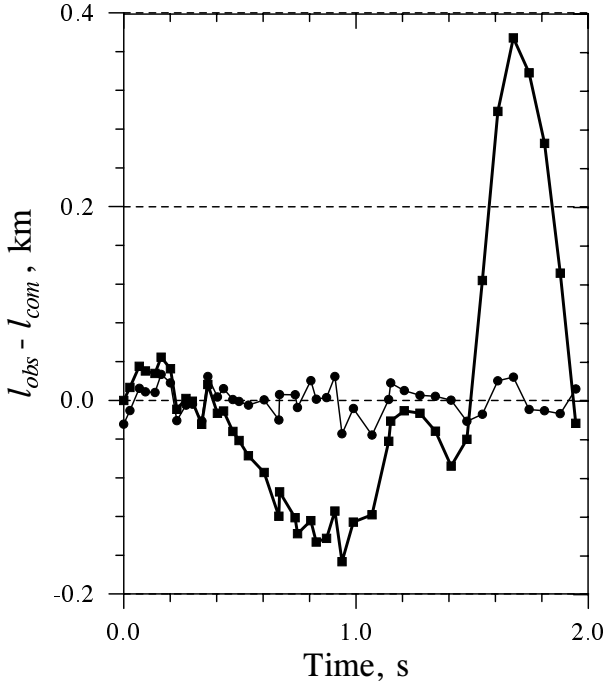

Fig. 2. Comparison of the length along the meteor trajectory as a function of time determined in the simulation ($l_{\rm com}$) and directly observed ($l_{\rm obs}$). The length difference obtained in the simulation with the radiative radius approach is shown by the thick line. The squares represent individual length measurements (shutter breaks). The values of $l_{\rm obs} - l_{\rm com}$ determined by fitting the observational data by the gross-fragmentation model are given by a thin line with circles. The zero point of the relative time was set at altitude 51.2 km

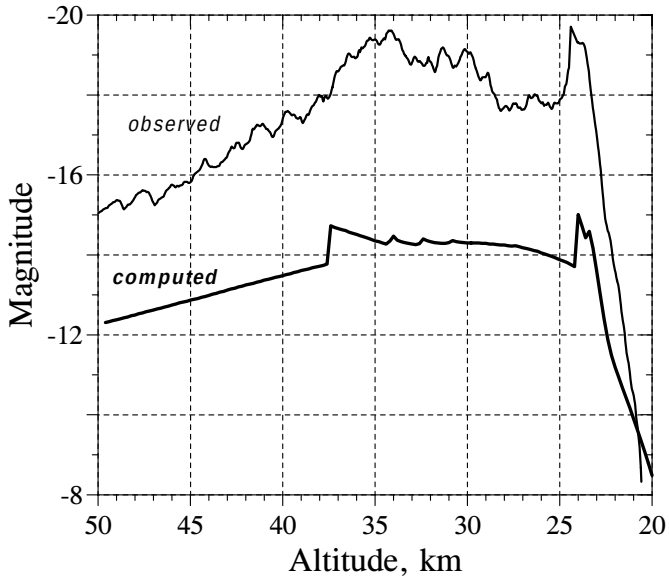

Fig. 3. The comparison of the observed light curve and the light curve computed on the basis of the dynamical solution and the luminous efficiency as given in the text

At first sight, it seems that the gross-fragmentation model of Ceplecha et al. (1993) describes the bolide better. It fits the dynamics below altitude 50 km quite well. However, if we look at the parameters of the model, we find that the initial meteoroid mass in the final solution is only 82 kg for an assumed density 3.7 g cm^{-3} or 280 kg for $\rho = 2$ g cm^{-3}. This low mass is quite understandable considering the fact that the meteoroid was significantly decelerated already at altitudes between 40 and 50 km. However, this mass is in strong discrepancy with the extreme brightness of the bolide. The initial photometric mass was determined to be 5000–13,000 kg by Borovička & Spurný (1996). Even if we considered an unrealistically high luminous efficiency of the order of 30% and possible errors in photometry, the initial meteoroid mass could not be lower than 1000 kg.

To display the difference between dynamic and photometric mass, the computed and observed light curve were plotted (Fig. 3). The computed light curve includes the luminosity of the main body and the observed fragments (see Sect. 4), summed at each altitude, and the contribution of the dust released at each fragmentation event and evaporated in a short time interval. The dust was simulated as a fragment with an ablation coefficient of 0.08 s^2 km^{-2}. The empirical luminous efficiency was used in this case (see Eq. (1) below).

The observed and computed light curve between 50 and 20 km show some common characteristics but the predicted brightness is much lower than observed. At 50–45 km and around 28 km, where probably no fragmentation occurred, the difference is about 3 mag, i.e. the photometric mass loss is 10–20 times higher than the mass loss rate derived from the dynamics. The beginning of fragmentation at about 45 km initiated a steeper increase of brightness than predicted. A violent fragmentation between 37–29 km and around 24 km produced bright maxima, with larger amplitude and width than predicted, indicating that much more dust was present and enhancing the discrepancy between the total dynamic and photometric mass.

Some parameters are free in the gross-fragmentation model. The ablation coefficient, drag coefficient, meteoroid density and shape are assumed to be constant. The product of the drag coefficient and the shape coefficient was assumed to be $\Gamma A = 1.2$ which means a relatively flat body considering a realistic value of $\Gamma \sim 0.7$. The size of the meteoroid decreases due to ablation and fragmentation. The mass was computed assuming a density of 3.7 g cm^{-3}. For 2 g cm^{-3} the resulting initial mass would be 280 kg. To obtain 5000 kg, an unrealistically low density of 0.5 g cm^{-3} would be needed. We consider this density unrealistic because the bolide penetrated deep into the atmosphere, survived a relatively large dynamic pressure of 90 Mdyn cm^{-2} and very probably produced meteorites. The body was almost certainly an ordinary or carbonaceous chondrite, so the density was not lower than 2 g cm^{-3}.

In summary, the gross-fragmentation model does not provide a self-consistent solution for the Benešov bolide. There is an order-of-magnitude difference between the dynamic and photometric mass. The radiative radius model is based on the light curve analysis, so the light is explained automatically. The dynamics is explained relatively well above 24 km, neverthe-

less also in this case the real deceleration between 40–50 km is larger than modeled. Moreover, the physical reasons for the substantial increase in effective radius are to be established.

Probably, the high intensity radiation at the altitudes of about 50–40 km is determined by the motion of a large number of fragments; that motion is somehow equivalent to the motion of a large low density single body with radius 60–80 cm, increasing to 100–150 cm due to aerodynamic loading and spreading at low altitudes (below 40 km). The largest surviving fragment determines the dynamical mass. The real mass of the Benešov meteoroid is much larger than its dynamical mass, and that is probably caused by its fragmentation at high altitudes. We will discuss this scenario in Sect. 5.

3.1. Bolide PN 39434

The Benešov bolide is not an exceptional one. There are some other bolides for which there is a great difference between dynamic, photometric and radiation masses. Another big bolide demonstrating such discrepancy is PN 39434, registered by the Prairie Network. It was a bright (-14 mag) bolide, although less intensive than the Benešov one and has a lower initial velocity 14.2 km s^{-1}. The divergence between the dynamic and photometric masses reaches about 70 times. The photometric mass is about 2000 kg, the dynamic mass is less than 30 kg (for $\rho = 3.7$ g cm^{-3}). This bolide had a rather high intensity and begun to decelerate at high altitudes (of about 50 km), as Benešov did.

Our estimates with the help of radiative radius approach is less than photometric one (by a factor of two), but greater than dynamic one by a factor of about 40. The resulting density is too low to be physically realistic for a body that has penetrated so deeply. The estimate of the radiative radius for this bolide is rather large (about 80–100 cm) at altitudes 40–50 km, it decreases with decreasing height (in contrary to Benešov) probably due to ablation, up to the terminal small increase. The pressure loading is smaller than that for Benešov bolide; its maximum is about 22 Mdyn cm^{-2}.

The earlier beginning of deceleration and the high value of the radiative radius may be arguments for the existence of a really big radiative volume due to early disruption. Attempts to reproduce simultaneously light and deceleration curves of this bolide in the framework of a single-body model run into the same problems as for Benešov: a rather high intensity at the end of trajectory simultaneously with rapid deceleration causes assumption of a low density for the bolide. So this bolide is probably caused by a body which was fragmented at rather high altitudes and later was flying as a swarm of fragments.

In the next section we will analyze the geometry and dynamics of individually observed fragments to obtain more data on the fragmentation of Benešov meteoroid. The data given here extend and update the information given in Borovička & Spurný (1996).

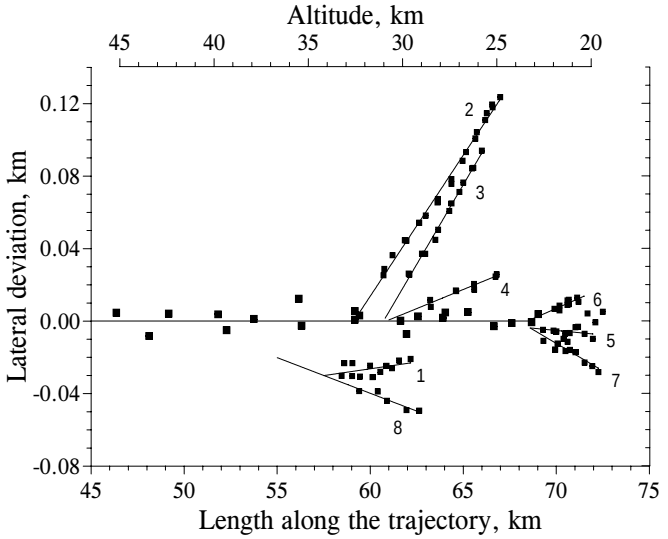

Fig. 4. The measured geometry of eight individual fragments of Benešov bolide. The individual positional measurements are given as squares. Larger squares belong to the main body. Note the highly enhanced scale on the y-axis. The lateral deviation represents in fact the projection to the plane perpendicular to the line of sight

4. Direct observational evidences of Benešov fragmentation

The fragments of the Benešov bolide were studied on the spectral record covering the lower part of the bolide trajectory. There are two regions of fragmentation. Five fragments are visible around altitude 30 km. These fragments deviate from the main trajectory and are all much fainter than the main body. They were measured on the zero spectral order. Some information on velocity was obtained for four of the fragments.

Below altitude 23 km the main trajectory splits into three measurable individual trajectories. As the zero order image is out of the field of view below altitude 21 km, the end of the fragment trajectories were measured on the sodium line in the first order spectrum. The sensitivity is lower in the first order and it can be expected that the fragments would be visible to lower altitudes on the zero order than on the first order. The bolide was visible down to 17 km in the fish-eye image where the individual fragments cannot be resolved.

The geometry of all fragments is displayed in Fig. 4. The positional measurements of the fragments are given with the lateral distance scale highly enhanced. Straight lines are drawn through the measured points. There seems to be a cyclic trend in the positions of fragment 2, but it is probably insignificant. In fact, the lateral deviations are projections on the plane perpendicular to the line of sight from Ondřejov. Around altitude 30 km, the fragments could be separated only if they deviated laterally at least 20 meters from the bright main body. Only if they were visible in the shutter breaks was a smaller deviation sufficient (fragment 4).

In Table 3, some data for individual fragments as derived from Fig. 4 are given. The separation altitude and the angle of separation were determined from the intersection of the trajectories of the fragment and the main body. The first detection

Table 3. Individual fragment data

Fragment No.	1	2	3	4	5	6	7	8
Separation height [km]	–	32.6	31.0	30.9	27	23.4	23.8	42
±		0.1	0.1	0.5	5	0.6	0.5	2
Separation angle [deg]	–	0.89	1.00	0.24	0.06	0.25	0.35	0.23
±		0.02	0.02	0.03	0.05	0.07	0.06	0.04
First detection [km]	33.3	31.1	29.8	28.5	22.6	22.6	22.6	33.8
Last detection [km]	29.5	24.8	25.7	25.0	19.9	19.4	19.6	29.1
Relative brightness	4	5	3	4	15	20	20	1
Theoretical separation angle* [deg]	–	0.16	0.17	0.17	0.25	0.32	0.28	0.077

* see Sect. 5.5

means the altitude at which the fragment was first seen as a separate piece. The last detection is where the fragment disappeared. Fragment 1 is peculiar because it moves toward the main trajectory. The last detection of fragment 1 is where it approached the main body too closely to be separated. Fragment 1 was probably derived not from the main body but from fragment 8. Fragment 8, however, is much fainter than fragment 1. The approximate relative brightness of fragments as estimated from the visual inspection of the negatives is also given in Table 3.

The separation heights show that fragments 3 and 4 were probably formed at the same point at the altitude of 31 km and fragments 5, 6, 7 have their common origin at the main body breakup at the altitude of about 24 km. The separation angle for different fragments is up to 1 degree. It means a maximum lateral separation velocity of the order of 300 m s^{-1}. Due to the projection geometry, this is a lower limit.

In addition to the geometry, time marks could be measured on most fragment trajectories. A good velocity profile is available for fragments 2, 3, 6, 7 and some information on the velocities of fragments 1, 5, 8 was also obtained. The gross-fragmentation model of Ceplecha et al. (1993) was applied to the time marks (i.e. shutter breaks) to obtain dynamical data on the fragments.

The dynamics of fragment 6 were solved together with the main body below altitude 55 km. A single-body solution produced a large systematic trend of residuals. Nevertheless, a fragmentation solution was found which removed the system completely (see Fig. 2, thin line). The fragmentation point could be found with a precision to one shutter break in this method. It was found to occur at altitude 23.5 km. This is in agreement with the geometric solution (see Table 3). The ablation coefficient in the fragmentation solution is 0.007 s^2 km^{-2}. The resulting initial dynamic mass of the main body of 82 kg is unrealistically small with regard to the bolide luminosity as discussed above. At the fragmentation point, the dynamic mass decreased from 31 kg to 5 kg.

The same procedure as for fragment 6 was followed for fragment 7. The fragmentation point was found one shutter break earlier, at 24.2 km. This is consistent, within the error, with the common origin of fragments 6 and 7. Nevertheless, the possibility that fragment 7 was separated a few hundred meters higher (a few hundredth of a second earlier) than fragment 6, as suggested by both the geometric and dynamic solution, remains. The ablation coefficient in the solution for fragment 7 is 0.006 s^2 km^{-2}.

The gross-fragmentation model was able to find the major fragmentation point correctly. The presence of other fragmentations was also suggested by the existence of a so called unrealistic solution (see Ceplecha et al. 1993) but the standard deviation of the fit was higher in this case and Benešov could therefore be classified as a bolide with one major fragmentation. The model also provided a reasonable ablation coefficient but the initial mass is in severe contradiction with the photometric mass.

Fragments 2 and 3 were solved separately. In both cases a single body solution with low ablation coefficient (0.0025 and 0.0015 s^2 km^{-2}, respectively) was found. Surprisingly, when extrapolating the velocity to the separation height, it was found that the velocity was much lower there than the velocity of the main body at the same height. This must be interpreted to mean that fragments 2 and 3 were not separated directly from the main body but from some undetected primary fragments which followed the trajectory of the main body but were more strongly decelerated. The separation height of the primary fragments is not known, but when inspecting the light curve, a relatively steep increase of brightness at 37.5 km is found. We succeeded in forming a consistent fragmentation sequence assuming that three primary fragments separated at 37.5 km and the observed fragments 1 to 4 and 8 were produced by secondary fragmentation of these primary fragments.

The situation is shown in Figs. 5–7. In Fig. 5 the velocities of all fragments are given as a function of altitude. The ablation coefficient 0.002 s^2 km^{-2} was assumed for the hypothetical fragments. The heights of the secondary fragmentations were known from the geometry. The velocities at those points were obtained by the backward extrapolation of the velocities fitted to the observed secondary fragments. The initial masses of the primary fragments were adjusted to obtain the desired velocity at the secondary fragmentation points.

The data on the fragments are presented schematically in Fig. 6. The dynamic masses, ablation coefficients, velocities, fragmentation heights and computed theoretical brightness are given. The dynamic masses were computed for an assumed den-

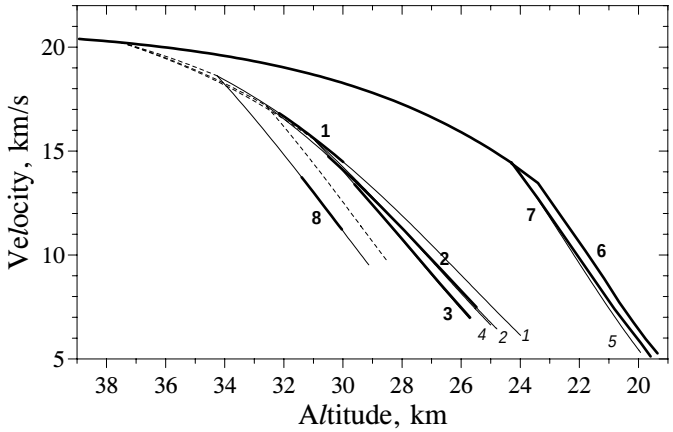

Fig. 5. Velocity curves of the fragments of Benešov bolide as determined from fitting and extrapolation by the gross-fragmentation model. The thick segments represent the intervals where the velocity was measured. Thin solid lines represent the extrapolation of fragment velocities and the dashed lines belong to hypothetical fragments not directly seen

sity of 3.7 g cm^{-3}. The brightness was computed schematically from the luminosity equation including the deceleration term:

$$I = -\tau(v)\left(\frac{v^2}{2}\frac{\mathrm{d}m}{\mathrm{d}t} + mv\frac{\mathrm{d}v}{\mathrm{d}t}\right) \quad (1)$$

The magnitude $M = -2.5\log I$ is given in Fig. 3. For the luminous efficiency the value $\log\tau = -12.99 + 0.106v$ was assumed for $v < 13$ km s^{-1}, $\log\tau = -11.90 + 0.022v$ for $13 < v < 17$ km s^{-1}, and $\log\tau = -11.59 + 0.0033v$ for $v > 17$ km s^{-1} which corresponds to 0.5% for 5 km s^{-1}, 1.8% for 10 km s^{-1} and 4.5% for 20 km s^{-1}. Due to the low ablation coefficient, the deceleration term produced most of the predicted luminosity. The fragments 2, 3, and 8 ceased to be visible when their computed magnitude was about -6. This enabled us to estimate the mass of fragment 4 and the terminal height of fragment 1, both quantities not directly derivable from observations. For fragments 5–7 the sensitivity limit is somewhat higher due to their observations in the first order spectrum. The actual magnitudes of the fragments could not be measured due to their vicinity to the main body and to the strong overexposure of the original negative.

The fragmentation sequence presented here is, of course, only one possibility to explain what was seen. Many more fragments probably existed which could not be identified on the negative. In addition, not only macroscopic fragments but also some tiny particles and dust must have been released at each fragmentation point. This is expressed in Fig. 6 by the fact that the total mass of the produced macroscopic fragments is always lower than the mass of the body before fragmentation.

Fig. 6 should be understood rather as a table schematically presenting the data and not having the correct scaling. Better impression of the fragmentation process can be obtained from Fig. 7. Here the fragments are displayed in true geometrical positions relative to the main body at nine different instants of time.

5. Modeling the fragmentation

The disagreement between the values of the dynamical mass, photometric mass and the mass from the radiative radius makes it necessary to continue the analysis. We shall try to fit the observational data on the velocity and light intensity assuming that the flight and radiation of several fragments is governed by the well-known system of equations of meteor physics (see e.g. Bronsten 1983) with some additional assumptions on fragmentation. Our aim is not to develop a new and quite general model but to demonstrate that severe early fragmentation can account for the observed discrepancies.

5.1. Modes of fragmentation

There are different models of meteoroid breakup (Svetsov et al. 1995). The liquid-like (hydrodynamic, "pancake") models imply that the heavy fragmentation takes place in the whole meteoroid which continues its flight as a single body with increasing cross-section. There are slightly different equations for velocity of radius growth in the literature (Svetsov et al. 1995); we shall assume that the velocity of radius increase U may be written as follows:

$$U = K_1 v\sqrt{\rho_a/\rho} \quad (2)$$

where v is the velocity of the body, ρ is the density of the body, ρ_a is the atmospheric density and K_1 is a constant. A heavily fragmented body may be treated as a cloud of small fragments and vapor.

On the other hand, the models of progressive fragmentation suppose that individual fragments are separated, i.e. fragments rapidly move apart and then travel independently from one another. Fragments may be also disrupted again in deeper atmosphere layers.

The real distribution of fragments on mass and their relative positions and interaction after a breakup are unknown. The mass distribution determined in experiments of catastrophic disruption (Fujiwara et al. 1989) was therefore used:

$$\mathrm{d}N/\mathrm{d}m = Cm^{k/3-2}, k = 1.2 \quad (3)$$

The recovered fragments of the H-chondrite Mbale meteorite (Jenniskens et al. 1994) also were described by this distribution.

If we assume first fragmentation into a big number of fragments and one or several fragmentation stages at lower altitudes we cannot avoid the problem of aerodynamic interaction between a large number of small fragments. This problem is a very complicated one even if we know the number and shape of the fragments formed. But this is not the case, so we shall use a simplified model.

According to estimates by Passey & Melosh (1980), Melosh (1989), and numerical simulations by Artem'eva & Shuvalov (1996) the lateral velocity appearing after fragment formation is

$$U = K_2 v\sqrt{\rho_a/\rho} \quad (4)$$

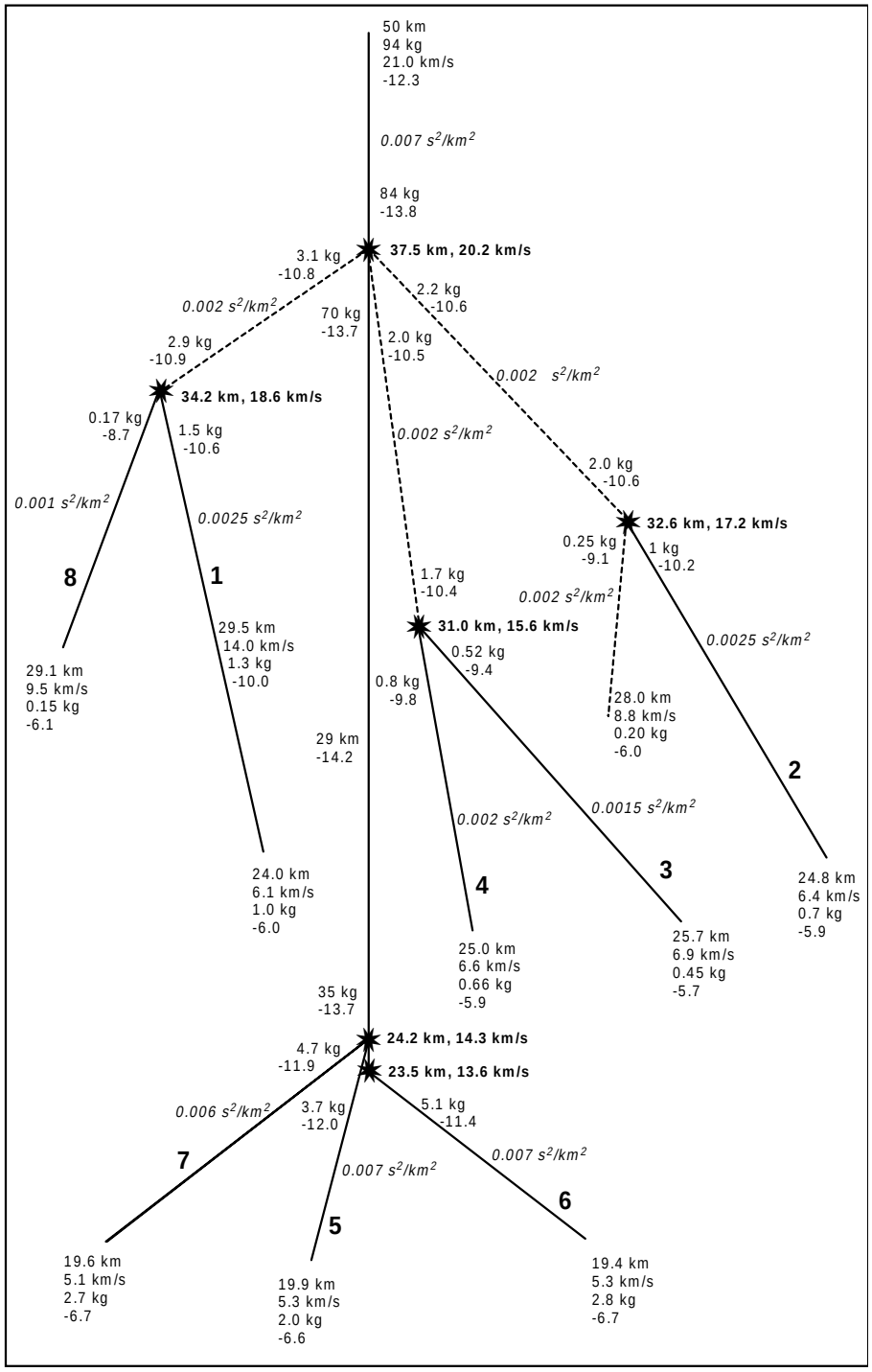

Fig. 6. The probable hierarchy of Benešov fragmentation. The dynamic data (altitude, mass, velocity, ablation coefficient) and derived theoretical magnitudes of individual fragments and the main body are given. The geometry is only schematic

where the value of K_2 depends on the number and shape of the fragments and may be estimated as $K_2 \sim 0.1$–1.2 for fragments with equal masses (Artem'eva & Shuvalov 1996; Passey & Melosh 1980). This law is equivalent to Eq. (2) for the velocity of radius increase in the liquid-like model. The interaction between the fragments practically disappears for a distance between fragments larger than about two times the size of the fragments.

5.2. Coefficients used

In the analysis of the Lost City meteoroid the combination of drag coefficient Γ and shape factor A was estimated as $\Gamma A \sim 1.1$ (Ceplecha 1996). A similar value ($\Gamma A = 1.2$) was also used in evaluating the dynamical mass and deceleration. For a spherical body this value is about 0.6, for a cubic cylinder ($L = 2R$) $\Gamma A \sim 0.92$, for a flat cylinder ($L = R$) $\Gamma A \sim 1.46$. In order to get a better agreement with the deceleration curve, the cylindrical

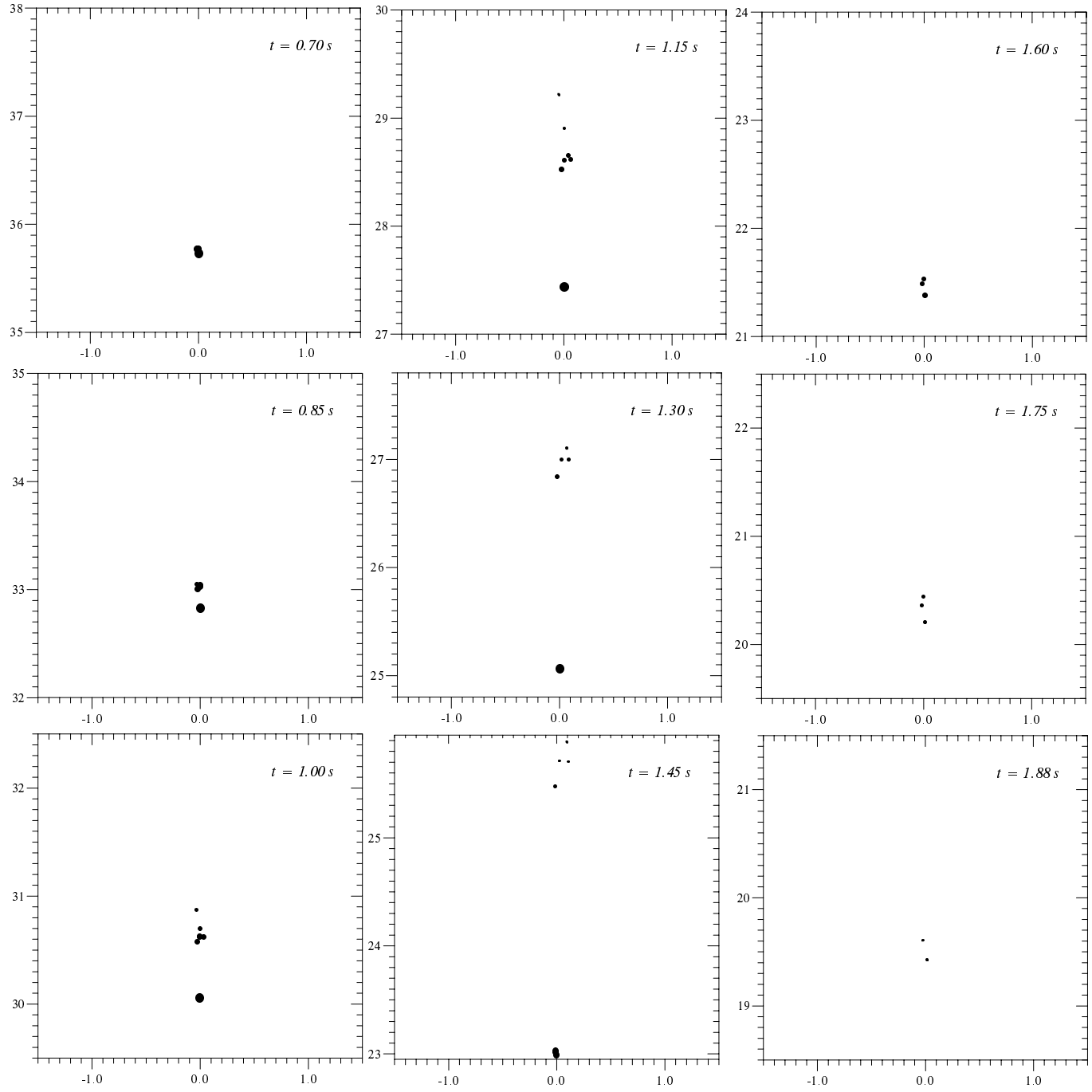

Fig. 7. Video-like view of observed Benešov fragmentation. The positions of fragments as visible from Ondřejov at fixed time instants are shown. The altitude is plotted on the vertical axis in each panel. The distance from the main trajectory is on the horizontal axis. The size of the symbols is proportional to the theoretical magnitude of the fragment. The time is counted from the passage through altitude 50 km

shape with $L = 1.5R$ ($\Gamma A \sim 1.12$) was assumed for both the unfragmented meteoroid and the fragments after breakup.

For the luminosity and ablation rates, theoretical values given in Tables 1 and 2 were used. The ablation coefficients determined with the help of the gross-fragmentation model varied from 0.0015 up to 0.007 s^2 km^{-2} for different fragments and the main body (Fig. 6). These values are comparable or lower than the theoretical values. They are lower than the typical ablation coefficient of type I bolides. We prefer to use in the following the theoretical values with their theoretical dependencies on altitude, velocity and size. The luminous efficiencies and ablation coefficients for small fragments outside the range of Tables 1 and 2 were obtained by extrapolation.

For the coefficient K_1 in Eq. (2) various values were tried. Finally, when fitting the observed light curve of Benešov, the value of 0.3 proved to be the best. K_2 was set to unity.

5.3. High altitude fragmentation

We cannot avoid the discrepancies in the deceleration at higher altitudes considering a single-body meteoroid with high enough mass. We therefore consider the possibility of high-altitude fragmentation.

At altitude 50 km the pressure at the blunt nose of the body reaches 5 Mdyn cm^{-2}; this is a typical breakup pressure of meteoroids (Ceplecha et al. 1993). The Benešov bolide is one of the largest bolides detected by the ground-based photographic network. The larger the size of the impacting body the easier it is to find a fault or a crack leading to fragmentation under the aerodynamic loading. Thus we anticipate that the breakup pressure may be as low as 1–5 Mdyn cm^{-2} and the first breakup may have occurred at an altitude of about 50–60 km. This value belongs to the lower half of typical pressure values causing gross fragmentation of PN bolides studied (Ceplecha et al. 1993). We cannot even exclude that the bolide was initially a tight swarm of loosely bound fragments.

We do not see fragments separating from the main body at high altitudes due to their rather low lateral velocity. According to estimate (4) at altitude 50 km ($\rho_a \sim 10^{-6}$ g cm^{-3}, $\rho = 2$ g cm^{-3}) the lateral velocity $U = \frac{1}{1400} v$ for $K_2 = 1$. For $v = 20$ km s^{-1} we have $U = 14$ m s^{-1}. The space resolution of the ground-based photographic system of observations is not better than +20 m, so one cannot detect fragments deviating from the main trajectory for more than 1 sec and cannot discriminate if a single body or a swarm of fragments are moving along the trajectory.

No flare which could be associated with the assumed breakup is present in the light curve at altitudes 50–60 km. This suggests that only large fragments have been formed or, at least, that small quickly evaporating dust constitutes only a small fraction of the mass. The absence of small fragments decelerated significantly behind the main body is confirmed by the absence of visible trails in the shutter breaks.

The aerodynamic interaction between the fragments practically disappears for a distance between fragments larger than about two times the size of the fragments, which is no more than 1 meter. Thus aerodynamic interaction between fragments becomes negligible in a fraction of a second.

An estimate of pressure loading mentioned above allows us to suppose that the meteoroid fragmentation occurred at higher altitudes. In this case at medium altitudes the intensity may be the sum of the light emitted by a swarm of fragments, and the deceleration relates only to the leading fragment.

5.4. Progressive fragmentation

After the high altitude breakup, further fragmentation events certainly followed. It is therefore possible to consider Benešov in the frame of the progressive fragmentation model (such a model has already been used by Popova & Nemtchinov (1996b) for the Sikhote-Alin iron shower). The fragments were divided into five mass bins after the first breakup and further simulations were done only for a representative fragment mass in each bin.

The radiation radius and light curve of Benešov allow us to suggest the existence of breakup points at altitudes of about 40–35 km. So, some part of the fragments was disrupted at these heights. Another part with the mass of the leading fragment, close to the dynamical mass estimate (of about 280 kg for $\rho = 2$ g cm^{-3}) survived up to the last catastrophic disruption at the altitude of 24 km, where a cloud of vapor and small fragments was evidently formed.

We supposed that the strength of the fragments formed (except the leading ones) increases proportionally to the relation between fragment mass and mass under disruption to the power α. The exponent α is about 0.4–0.5 (Svetsov et al. 1995). The altitude of breakup was a prescribed value for leading fragments. The leading fragment with a mass corresponding to dynamical estimates is the biggest one. The considered mass range of fragments is rather small because it was necessary to get agreement with the deceleration curve.

One possible scenario is shown in Fig. 5.4. The meteoroid, with initial mass of 4000 kg, and bulk density $\rho = 2$ g cm^{-3} disintegrates at 56 km height. The distribution of fragments over mass in the first breakup is shown in Fig. 8a by squares. The body may fragment into 25 pieces with mass from 100 up to 280 kg under the breakup pressure of about 2 Mdyn cm^{-2}. Later at altitudes of about 39–32 km most of these fragments may break up under a pressure loading of about 25–30 Mdyn cm^{-2} into a large number of relatively small pieces (with a mass of about 1–10 kg) (stars in Fig. 8a) and some of them are fragmented once more at lower altitudes. The fragments from different bins break up at slightly different heights due to mass difference. The resulting small pieces decelerate more rapidly than the unfragmented part of mass (Fig. 8b), which survives until break-up into a spreading cloud at 24 km. About 800–1000 kg of total mass suffers the last fragmentation.

The resulting light curve is shown in Fig. 8c in comparison with the observed one. Successive fragmentation allows us to reproduce the growth of intensity in the light flare at altitude about 40–35 km although it doesn't describe the first intensity maximum wholly satisfactorily. The shape of the light pulse depends on the assumed distribution of fragments over mass. The light intensity rises more sharply if fragments of smaller sizes are formed in every breakup.

Different configurations of fragments may appear after a breakup due to their hydrodynamic interaction (Artem'eva & Shuvalov 1996). The fragments formed may interact with each other. The interaction of a large number of small fragments may lead to the creation of a cloud of small fragments and vapor preceded by a common bow shock wave. It is probable that such a cloud of fragments was formed not only at the altitude of 24 km, but at 40–35 km, too. For its description we shall use the liquid-like model.

It was assumed again that the first fragmentation height was about 55 km and that the mass distribution at this altitude was the same as in the previous example (Fig. 8a). The independent clouds of vapor and small fragments were formed during the next fragmentation stage at altitudes below 40 km. Some of the first-stage fragments are flying unbroken up to the final breakup

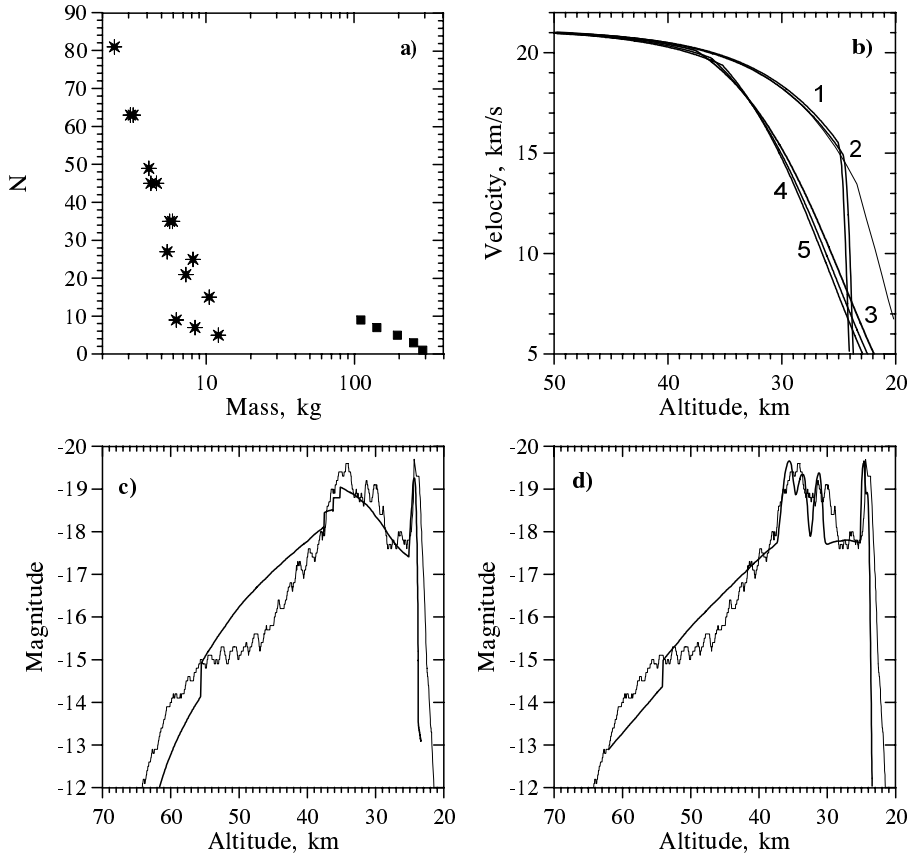

Fig. 8a–d. Modeling the Benešov bolide with the progressive fragmentation model. **a** Distribution of fragments by mass at the breakup moments (squares – at 60 km altitude, stars – at 40–36 km). The initial mass is 4000 kg, **b** Deceleration curves of various modeled fragments and of the observed main body (thin line), **c** Modeled (thick line) and observed (thin line) light curve, **d** Same as c) but under assumption that disruption at the 39–35 km altitude created clouds of fragments and vapor and that the initial mass was 3000 kg

at altitude 24 km. To get a better agreement with the flare amplitude, the initial mass of Benešov was assumed to be 3000 kg in this case. The mass disintegrated in the last fragmentation event is about 1200–1500 kg. The resulting light curve is shown in Fig. 8d. It is in general agreement with the observed curve. The two peaks of the first flare are produced due to the assumption of different breakup heights for different mass bins.

In summary, the progressive fragmentation model together with some additional assumptions allows us to reproduce the light and deceleration curve simultaneously. The mass estimate for the Benešov meteoroid is about 3000–4000 kg for a bulk density of 2 g cm^{-3}. The decrease of bulk density decreases the radius of fragments and increases the number of pieces.

5.5. Fragmentation details

In this section we compare some results of the progressive fragmentation model with the data on the observed fragments (Sect. 4). We should, however, keep in mind that only fragments sufficiently separated from the main body could be observed and these form only a minority of the existing fragments.

The size of the cloud of vapor and small fragments in the model is defined by the largest fragments in the cloud. They determine the divergence angle of the cone, while smaller fragments and the vapor are filling this cone and are entrained into the wake of the leading fragments. Deceleration is determined by the total mass of the cloud, while the angle of divergence is determined by the processes at the moment of fragmentation. That is the main difference between the simple pancake model and our approach, which we may call the model of the cone-like diversion of the cloud of fragments and vapor stabilized by the largest solid fragments.

According to Eq. (4) it is possible to estimate the separation angles for fragments formed at different altitudes. Separation angles computed by using Eq. (4) in assumption $\rho = 2$ g cm^{-3} and $K_2 = 1$ are compared with the observed angles in Table 3. One might expect an increase of angle with the increase of the air density. But no systematic trend in the deviation angle is present.

For three fragments at altitude around 30 km the observed angles are of the same order of magnitude as the theoretical ones. For two other fragments they are bigger by a factor of 6. According to Passey & Melosh (1980), Eq. (4) should be modified by a factor of $(M/m_f)^{1/2}$, taking into account the relation between the fragment masses m_f and the mass of the main body M. If $M \gg m_f$, this may increase substantially the theoretical separation angles. However, according to our interpretation in Fig. 6, fragments 2 and 3 were formed by a secondary disruption into pieces of the same order of mass. Their large separation angle was more probably caused by their peculiar shape among lots of ordinary fragments. The apparent cyclic trajectory of fragment 2 (Fig. 4) may support this idea. At lower altitudes, around 25 km, fragments are observed to

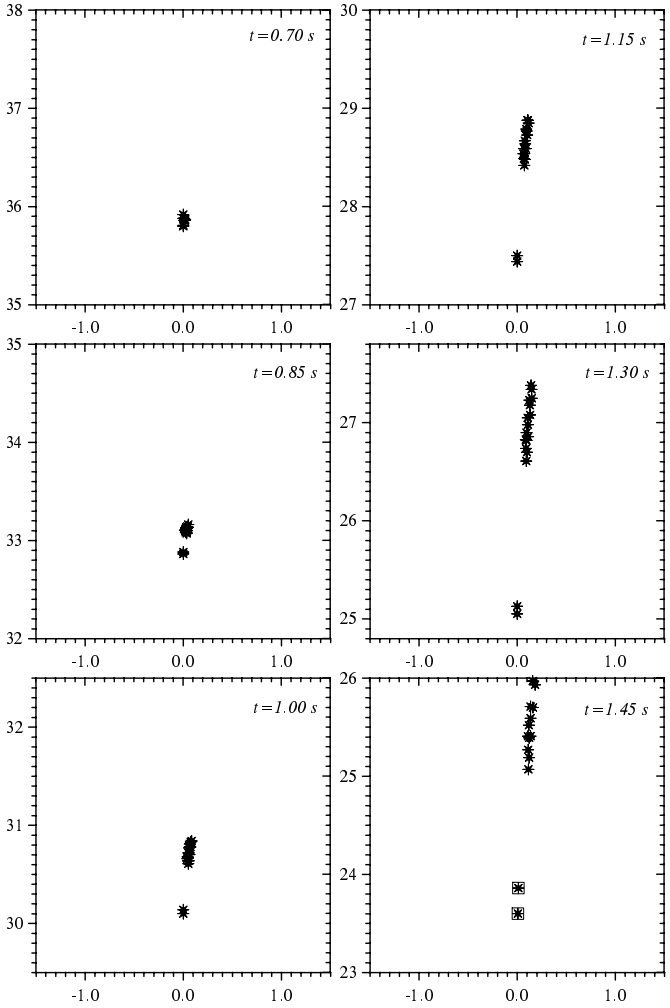

Fig. 9. Video-like view of modeled Benešov fragmentation. The altitude is plotted on the vertical axis, and the distance from the main trajectory is on the horizontal axis. The time is counted from the passage through altitude 50 km. The size of symbols is not connected with the relative brightness of the fragment groups. Only at the last instant the two brightest groups are marked also by squares. Compare to Fig. 7

deviate at an angle of about 0.25–0.3° in agreement with the predicted values.

As far as the other parameters are concerned, the calculated fragment velocities at altitude about 25 km are about 6–9 km s^{-1}, fragment masses are about 1.4–7 kg (or about 0.4–2 kg for $\rho = 3.7$ g cm^{-3}). These values are also close to the dynamic estimates given in Fig. 6. It should be remembered, that the dynamic mass estimates given in Fig. 6 were obtained for an assumed bulk density of 3.7 g cm^{-3}.

The modeling video-like pictures are demonstrated in Fig. 9 at the same moments as for the observed one (Fig. 7). Separated fragments were not considered in the last catastrophic fragmentation, so the last three instants were excluded. Every star corresponds to some group of fragments. The position of the fragments at different times are close to the observed positions, although the number of fragments is substantially larger in the modeling. The main difference appears at the last times considered, pointing out a difference in deceleration. This is probably caused by a difference in ablation rates. The main part of the fragments formed is small, and an extrapolation of theoretical luminous efficiencies should be used in estimates of radiation, so we do not compare the precise intensity for different fragments. Only at the last instant the two brightest groups of fragments are marked additionally by open squares. The estimated magnitude for some fragments is below -6 mag or -7 mag so they may have become invisible by that time. The lateral deviation was estimated by absolute value and supposed to appear in one direction, so the resulting picture has less symmetry than the observed one.

The description of meteoroid breakups presented is not a precise solution, many arbitrary parameters exist. Some rough approximations were used in the modeling. Nevertheless, comparison of these two video-like records allow us to conclude that they resemble each other rather closely.

6. Conclusions

Detailed analysis of the dynamics, fragmentation and light curve of one of the largest and well documented bolides – the Benešov bolide – has been performed. There is a large difference between the dynamic mass of about 80–300 kg and the photometric mass (5000–13,000 kg). This difference may be eliminated assuming low initial density of meteoroid ($\rho_0 \sim 0.5$ g cm^{-3}), but this assumption contradicts the deep penetration of Benešov bolide.

At altitudes of 39–34 km and below 25 km the radiative radius increases rapidly and this clearly indicates severe fragmentation at these altitudes. This fragmentation has been confirmed by direct observation of fragments deviating from the main trajectory. Nevertheless, this late fragmentation cannot account for the mass discrepancy.

It has been suggested that at altitudes of about 50–60 km the Benešov meteoroid has been already fragmented. Due to the low lateral velocity of the fragments at these altitudes, the fragments do not diverge to distances larger than 20 m laterally, which is the resolution of photographic measurements. Since only relatively large fragments are formed, no flare on the light curve is produced. The fragmentation cannot be detected dynamically, because of negligible change of deceleration at these altitudes. So neither method is able to locate the fragmentation point.

If the meteoroid is fragmented and fragments are flying individually the observed deceleration and dynamic mass are determined by the leading fragment, while the total mass of the fragments is larger than that of the leader. Thus usage of the light curves for mass estimates may give more reliable results than the dynamical analysis at least in some cases.

To describe the Benešov bolide completely, the progressive fragmentation model has been used. It was assumed that at altitudes of about 50–60 km a number of large fragments (10–30) has been formed with a mass of about dynamical mass estimate. The total mass is about 3000–4000 kg. The first breakup occurred when pressure is of the order of 1–5 Mdyn cm^{-2} and that doesn't contradict typical values of breakup pressure for

PN and EN bolides keeping in mind the rather large initial mass of Benešov.

Motion, ablation and radiation of all the fragments during some period of time has been described individually. Descending to lower altitudes, fragments continued to disintegrate (progressive fragmentation) due to increased aerodynamic loading. At altitude about 39–37 km gross-fragmentation of fragments occurred and bolide luminosity increased dramatically. Some compact fragments survived and were disrupted only at altitudes about 24 km under the dynamic pressure of 90 Mdyn cm^{-2}, causing a major flash. This final flash could be described in the framework of a liquid-like model.

It is likely that the disruption of the Benešov meteoroid was very complex (not pure pan-cake or progressive fragmentation models). Clouds of small fragments and vapor with a common shock wave were formed, but a number of fragments escaped from the common motion and moved individually. Some fragments deviated strongly and were observed directly. The fragments dynamics found as a result of numerical simulations is close to the observed one.

These assumptions allowed us to explain the discrepancy between the dynamics and radiation or between the dynamic and photometric masses and to reproduce the intensity and shape of the light curve.

The behavior of the Benešov meteoroid, its dynamics, breakup and light flash, is probably typical for big stony meteoroids. Smaller meteoroids start to fragment under similar pressures but there is not enough mass to form so rich a swarm of fragments with complex mutual hydrodynamics and several stages of disruption events.

The simplified indirect integration model used for the assessment of the SN bolide characteristics has been applied to the Benešov meteoroid and the resulting mass is about 2000 kg, which is close to the results of the detailed analysis using tracking of individual fragments and the progressive fragmentation model. This gives additional support for using the simplified model, if no further information is available.

We should note that in this paper the bolide was analyzed only below altitude about 60 km. The used hydrodynamic models cannot be applied to higher altitudes. The Ceplecha's gross-fragmentation model, when applied to the whole trajectory, failed to give a solution with non-systematic residuals. So, there exist some problems at higher altitudes as well. However, these problems are probably unrelated to the problems discussed here and the major aspect of the Benešov bolide which is the extensive fragmentation in several stages.

New more sophisticated theoretical models should be developed in the future for a more precise description of the atmospheric entry processes taking into account specific features found in the course of the study of the Benešov and some other EN and PN large bolides, i.e. increased ablation rate due to early fragmentation, turbulent mixing and turbulent diffusion, aerodynamic interaction between fragments following in the wake of the leader or side by side in a tense swarm etc. But at present, existing models, e.g. the ablating piston model including progressive fragmentation, seems to be a reasonable first estimate.

The analysis of the Benešov bolide will be continued in the subsequent paper, where theoretical and observed spectra will be compared. This comparison will provide additional information on the ablation and radiation processes.

Acknowledgements. This work is supported by grant no. 205-97-0700 from the Grant agency of the Czech Republic and by Sandia National Laboratories.

References

Adushkin V.V., Nemchinov I.V., 1994, In: Gehrels T. (Ed.) Hazards due to Comets and asteroids. Univ. Arizona Press, Tucson & London, p. 721

Artem'eva N.A., Shuvalov V.V., 1996, Shock Waves 5, 359

Biberman L.M., Bronin S.Ya., Brykin M.V., 1980, Acta Astronautica 7, 53

Borovička J., 1993, A&A 279, 627

Borovička J., 1994, Planet. Space Sci. 42, 145

Borovička J., Spurný P., 1996, Icarus 121, 484

Bronsten V.A., 1983, Physics of Meteoric Phenomena. D. Reidel Publ. Co., Dordrecht

Ceplecha Z., 1987, Bull. Astron. Inst. Czech. 38, 222

Ceplecha Z., 1996, A&A 311, 329

Ceplecha Z., McCrosky R.E., 1976, J. Geophys. Res. 81 (35), 6257

Ceplecha Z., Spurný P., Borovička J., Keclíková J., 1993, A&A 279, 615

Ceplecha Z., Spalding R.E., Jacobs C., Tagliaferri E., 1996, Sizes and masses of satellite observed meteoroids. In: Proceed. Comet Day II (5 th Intern. Conf. Space-96), June 1- 6, 1996, Albuquerque, New Mexico, 7p.

Chernyi G.G., 1959, Techeniya gaza s bol'shoi sverkhzvukovoi skorost'yu (Flows of gas with a high supersonic speed). Fizmatgis, Moscow (in Russian)

Fujiwara A., Cerroni P., Davis D., et al., 1989, In: Binzel R.P., Gehrels T., Matthews M.S. (Eds.) Asteroids II. Univ. Arizona press, Tucson, Arizona, p. 240

Givens J.J., Page W.A., 1971, J. Geophys. Res. 76, 1039

Golub' A.P., Kosarev I.B., Nemtchinov I.V., Shuvalov V.V., 1996a, Solar System Research 30, 183

Golub' A.P., Kosarev I.B., Nemtchinov I.V., Popova O.P., 1996b, Meteoritics Planet. Sci. 31, A52 (Supplement)

Golub' A.P., Kosarev I.B., Nemtchinov I.V., Popova O.P., 1997, Solar System Research 31, 85

Halliday I., Griffin A.A., Blackwell A.T., 1981, Meteoritics 16, 153

Hayes W.D., Probstein R.F., 1959, Hypersonic flow theory. Academic press, New-York and London

Jenniskens P., Betlem H., Betlem J., et al., 1994, Meteoritics 29, 246

Kosarev I.B., Loseva T.V., Nemtchinov I.V., 1996, Solar System Research 30, 265

Melosh H.J., 1989, Impact cratering: a geological process. Oxford Univ. press, Clarendon press, Oxford, New York, 245p.

Morrison D., Chapman C.R., Slovic P., 1994, In: Gehrels T. (Ed.) Hazards due to Comets and Asteroids. Univ. Arizona Press, Tucson & London, p. 59

Nemtchinov I.V., Popova O.P., Shuvalov V.V., Svetsov V.V., 1994, Planet. Space Sci. 42, 491

Nemtchinov I.V., Popova O.P., Shuvalov V.V., Svetsov V.V., 1995, Solar System Research 29, 133

Nemtchinov I.V., Loseva T.V., Teterev A.A., 1996, Earth, Moon and Planets 72, 405

Nemtchinov I.V., Svetsov V.V., Kosarev I.B. et al., 1997, Icarus 130, 259
Passey Q.R., Melosh H.J., 1980, Icarus 42, 211
Popova O.P., Nemtchinov I.V., 1996a, Meteoritics Planet. Sci. 31, A110 (Supplement)
Popova O.P., Nemtchinov I.V., 1996b, Meteoritics Planet. Sci. 31, A110–A111 (Supplement)
ReVelle D.O., 1979, J. Atmosph. Terr. Phys. 41, 453
ReVelle D.O., 1980, J. Geophys. Res. 85 (B4), 1803
Spurný P., 1994, Planet. Space Sci. 42, 157
Svetsov V.V., Nemtchinov I.V., Teterev A.A., 1995, Icarus 116, 131
Tagliaferri E., Spalding R., Jacobs C., Worden S.P., Erlich A., 1994, In: Gehrels T. (Ed.) Hazards Due to Comets and Asteroids, Univ. Arizona Press, Tucson & London, p.199